Extreme Mechanics Letters 51 (2022) 101592

Contents lists available at ScienceDirect

Extreme Mechanics Letters

journal homepage: www.elsevier.com/locate/eml

Deformation activated negative group velocity state in soft laminates

Nitesh Arora [a,*], Qi Yao [a], Stephan Rudykh [a,b]

[a] Department of Mechanical Engineering, University of Wisconsin–Madison, Madison, WI, USA
[b] School of Mathematical & Statistical Sciences, National University of Ireland Galway, Galway, Ireland

ARTICLE INFO

Article history:
Received 3 August 2021
Received in revised form 12 November 2021
Accepted 12 December 2021
Available online 22 December 2021

Keywords:
Metamaterial
Soft matter
Wave propagation
Instabilities
Group velocity
Shear waves

ABSTRACT

We report the observation of deformation-induced negative group velocity (NGV) state in the non-periodic media. The phenomenon is illustrated by examples of the shear waves traveling along the non-periodic direction of pre-strained soft laminates. We show that the NGV state can be induced in absolutely stable laminates without invoking buckling. These stable composites with activated NGV states are achieved through tailored stiffening behavior of their non-Gaussian soft phases. The deformation range – for which the NGV state is activated – is multiple times higher in the proposed absolutely-stable composites than those prone to buckling. Finally, we analyze how this unusual NGV state can be induced and further tuned by variations in the material and geometric parameter spaces.

1. Introduction

Acoustic metamaterials, a class of architectured composite media, allow us to engineer and control the propagation of waves. These materials exhibit intriguing or unusual physical phenomena, including negative phase [1–3] and group velocities [4], frequency filtering [5,6], cloaking [7], acoustic diode [8], among others. The left-handed behavior of these metamaterials originates from their peculiar microstructure, which can be predesigned to achieve desired functionalities. Furthermore, *soft* metamaterials can be designed to actively tune their acoustic properties through applied deformation [9–16].

In this work, we focus on the occurrence of an anomalous state of negative group velocity (NGV). In such a state, the material may exhibit left-handed behavior characterized by opposite signs of phase and group velocities. The behavior has been observed under extreme conditions, for example, in liquid Helium-3 (a Fermi-liquid) [17] and Helium-4 (a Bose-liquid) [18] at low temperatures. Recently, the occurrence of NGV has been demonstrated in an architectured 3D metamaterial [19]. The NGV state is often accompanied by unusual behaviors, including backward propagation of waves and co-existence of three different modes with the same polarization at one frequency. This left-handed behavior can be utilized for inducing negative refraction [20,21].

Here, we study the appearance of the NGV state for the transverse or shear (S) waves in soft layered composites (LC). Remarkably, the NGV state can be induced for the waves traveling along the non-periodic direction of the composite, i.e., in parallel to the layers [see Fig. 1]. Moreover, the transition from positive to negative group velocity is not accompanied by significant geometrical changes and can be reversibly controlled by applied deformation. Such transition in the acoustic state of soft composites has been reported to foreshadow elastic instabilities [22]. Here, however, we show that the NGV state is not necessarily followed by an elastic instability. In particular, we propose the design of *absolutely-stable* composites (not prone to buckling) exhibiting the left-handed behavior when compressed. As we shall show, the deformation range – for which the NGV state is activated – is multiple times higher in the stable composites as compared to laminates that develop instabilities. Therefore, these stable composites curtail the need to operate in the vicinity of elastic instability, together with a meaningfully larger NGV attainable deformation range. These properties altogether make the soft laminate a viable medium for achieving deformation-controlled switch from right to left-handed acoustic behavior.

2. Problem definition and modeling

Consider a periodic layered composite consisting of two alternating hyperelastic phases – stiff layer and matrix, as shown in Fig. 1. The volume fraction of the stiff layer is $c^{(f)}$ and that of the matrix phase is $c^{(m)} = 1 - c^{(f)}$. Here and thereafter, the fields and parameters for the stiff layer and matrix are denoted by $(\bullet)^{(f)}$ and $(\bullet)^{(m)}$, respectively. Geometrically, the thickness of the stiff layer is $c^{(f)}a$, where a is the period of the laminate in the reference configuration [see Fig. 1]. The constitutive behavior of the phases

* Corresponding author.
E-mail address: narora7@wisc.edu (N. Arora).

https://doi.org/10.1016/j.eml.2021.101592
2352-4316/

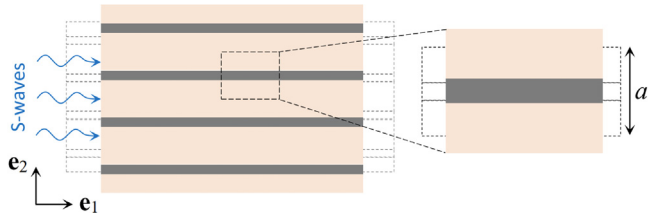

Fig. 1. Schematic of a deformed layered composite subjected to compression along the layers ($\mathbf{e}_1$-direction). The dashed boundaries in the background show the laminate in the undeformed state. The representative volume element (RVE) is shown on the right.

is defined by the Gent strain energy density function (SEDF) [23], namely,

$$\psi^{(r)} = -\frac{\mu^{(r)}}{2} J_m^{(r)} \ln\left(1 - \frac{\mathbf{F}^{(r)}:\mathbf{F}^{(r)} - 3}{J_m^{(r)}}\right) + \frac{\kappa^{(r)}}{2}(J^{(r)} - 1)^2, \tag{1}$$

where $\mu^{(r)}$ and $\kappa^{(r)}$ denote the shear and bulk modulus of the phases, $r \in \{f, m\}$; $\mathbf{F}^{(r)}$ is the deformation gradient tensor, and $J^{(r)} \equiv \det \mathbf{F}^{(r)}$. Here, the locking parameter $J_m^{(r)}$ captures the stiffening behavior (arising due to, for example, finite extensibility of the polymer chains [24]). The phase locks up, leading to a significant increase in the stress levels as the deformation approaches the limiting deformation level, $(I_1^{(r)} - 3) \to J_m^{(r)}$. Here, $I_1^{(r)}$ is the first invariant of the right Cauchy–Green deformation tensor, $\mathbf{C}^{(r)} = \mathbf{F}^{(r)\top}\mathbf{F}^{(r)}$. To realize the absolutely-stable scenario in soft laminates, we consider the matrix phase possessing stiffening behavior and stiff layer to be non-stiffening [25]. To this end, we set a very high value for the stiff layer's locking parameter, $J_m^{(f)} = 10^3$. To model the *nearly incompressible* behavior of both phases, we set a high bulk-to-shear modulus ratio, $\kappa^{(r)}/\mu^{(r)} = 10^3$. The layered composite is subjected to in-plane deformation defined by the following homogeneous macroscopic deformation gradient:

$$\overline{\mathbf{F}} = \lambda \mathbf{e}_1 \otimes \mathbf{e}_1 + \lambda^{-1}\mathbf{e}_2 \otimes \mathbf{e}_2 + \mathbf{e}_3 \otimes \mathbf{e}_3, \tag{2}$$

where λ is the applied macroscopic stretch ratio and $\mathbf{e}_i$ are the basis vectors as shown in Fig. 1. The locking condition, $(I_1 - 3) = J_m^{(m)}$, together with the assumed deformation Eq. (2), yields the lock-up stretch for the Gent matrix subjected to compression ($\lambda < 1$), namely, $\lambda_{lock} = \sqrt{(J_m^{(m)} + 2 - \sqrt{J_m^{(m)2} + 4J_m^{(m)}})/2}$.

To study S-wave propagation in hyperelastic layered composites, we employ small amplitude motions superimposed on finite deformations [13,26–28]. The incremental equation of motion is

$$\mathrm{Div}\dot{\mathbf{P}} = \rho_0 \frac{D^2\mathbf{u}}{Dt^2}, \tag{3}$$

where operator $D^2(\cdot)/Dt^2$ represents the material time derivative, Div denotes the divergence operator with respect to the reference (or undeformed) configuration position vector $\mathbf{X}$, ρ_0 is the initial density, $\mathbf{u}$ is the incremental displacement. The incremental first Piola–Kirchhoff stress tensor is defined as $\dot{\mathbf{P}} = \mathcal{A}\frac{\partial \mathbf{u}}{\partial \mathbf{X}}$, where $\mathcal{A} = \frac{\partial^2 \psi}{\partial \mathbf{F} \partial \mathbf{F}}$ is the tensor of elastic moduli for a SEDF ψ. In particular, we implemented the small-amplitude motions in the form of Bloch waves $\mathbf{u}(\mathbf{X}, t) = \mathbf{U}(\mathbf{X}) \exp[i(\mathbf{K}\cdot\mathbf{X} - \omega t)]$, where ω is the angular frequency, $\mathbf{K}$ is the Bloch wave vector in the reference configuration, and $\mathbf{U}$ is a periodic function subjected to the periodicity condition $\mathbf{U}(\mathbf{X} + \mathbf{R}) = \mathbf{U}(\mathbf{X})$, $\mathbf{R}$ denote the spatial periodicity in the reference configuration. In the present work, we examine the wave propagation along the $\mathbf{e}_1$-direction, therefore, the Bloch wave vector is $\mathbf{K} = K_1\mathbf{e}_1$. The two-step Bloch–Floquet analysis is performed in COMSOL 5.4 as follows. First, the solution for finitely deformed periodic composite is obtained. Second, the Bloch–Floquet conditions are superimposed on the deformed state for each strain level and the eigenvalue problem associated with the wave equation is solved for various values of wavenumber K_1. Hence, for each strain level, we obtain the dispersion relation $\omega = \omega(K_1)$. The Bloch-wave vector in the deformed configuration, $\mathbf{k} = k_1\mathbf{e}_1$, is related to that in the undeformed configuration as $\mathbf{k} = \overline{\mathbf{F}}^{-\top}\mathbf{K}$.

Recall that the soft composites may develop elastic instabilities under deformation [29–34]. Following the instability analysis employed in previous studies [35–38], we utilize the dispersion relations obtained through Bloch–Floquet analysis to predict the onset of elastic instabilities. In particular, instability occurs at a critical deformation level for which $\omega(k_1) = 0 (k_1 \neq 0)$. Based on the corresponding wavelength of the buckling pattern, the instabilities can be classified into macroscopic (or longwave) and microscopic instability. Macroscopic instability is characterized by the critical wavelength significantly larger than the characteristic microstructure ($k_1 \to 0$), while microscopic instability leads to the formation of new periodicity of the order of initial microstructure.

3. Results

We start with analyzing the influence of the matrix phase stiffening on the instabilities and occurrence of NGV state in laminates. In Fig. 2, we plot the critical stretch λ_{cr} (blue circles) for laminates with initial shear modulus contrast $\mu^{(f)}/\mu^{(m)} = 10$ and $c^{(f)} = 0.02$ as a function of matrix locking parameter $J_m^{(m)}$. Here and thereafter, both phases have identical densities, i.e., $\rho^{(f)}/\rho^{(m)}$ (until stated otherwise). We observe that these laminates develop microscopic instabilities at higher values of the matrix locking parameter. Moreover, the stability of the composite increases (λ_{cr} decreases) with the increase in the stiffening of matrix phase (a decrease in $J_m^{(m)}$). Notably, a completely stable scenario is realized at smaller values of matrix locking parameter ($J_m^{(m)} < 1.12$). The region where instability is attainable ($J_m^{(m)} \geq 1.12$) is shaded in yellow. In this region, the composites also show the transition in group velocity from positive to negative at deformations smaller than the critical level; the corresponding stretch ratio is represented using orange triangles in Fig. 2. In this region, the deformation range for which NGV state is active is bounded by the composite's stability, hence, the NGV strain range is defined as $\Delta\varepsilon_{ngv} = \lambda_s - \lambda_{cr}$. This strain range, as the function of $J_m^{(m)}$, is highlighted by the checker-shaded area between the NGV onset (orange) and the critical stretch (blue) curves. We observe that similar to λ_{cr}, λ_s also decreases with the decrease in matrix locking parameter.

Remarkably, the left-handed behavior is even observed in some of the LCs that do not develop instability, $J_m^{(m)} < 1.12$. In particular, the NGV state is exhibited by LCs with $0.98 < J_m^{(m)} < 1.12$; this region is shaded in red [see Fig. 2]. In these composites, the slope of the dispersion curves turns negative at λ_s [see orange hollow triangles] and switches back to positive at stretch λ_e termed as NGV ends [see hollow red squares]. Note that in this region, the laminates are absolutely-stable, and the critical stretch does not exist, therefore, the NGV strain range is defined as $\Delta\varepsilon_{ngv} = \lambda_s - \lambda_e$ (highlighted by the checker-shaded area between the NGV onset and NGV ends curves). Clearly, the absolutely-stable composites belonging to this (red) region are characterized by wider NGV strain ranges as compared to those that develop instabilities (yellow region). We observe that with the decrease in $J_m^{(m)}$, λ_s decreases, whereas λ_e increases, thus overall, there is a decrease in NGV strain range. Subsequently, at very small values of matrix locking parameter ($J_m^{(m)} \leq 0.98$), the absolutely-stable

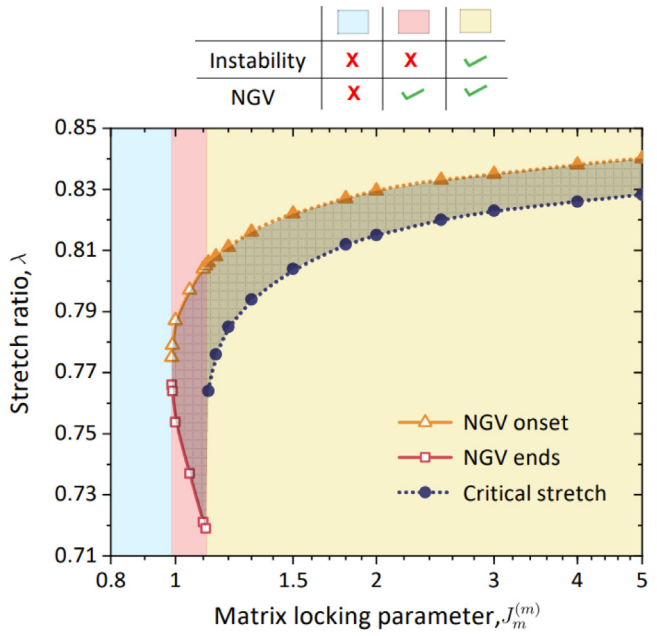

Fig. 2. Critical stretch (blue circles) and stretch ratios for the onset (yellow triangles) and end (red squares) of NGV state vs the matrix locking parameter $J_m^{(m)}$. The checker-shaded region between the two curves shows the NGV strain range $\Delta\varepsilon_{ngv}$. LCs with $\mu^{(f)}/\mu^{(m)} = 10$ and $c^{(f)} = 0.02$ are considered. (For interpretation of the references to color in this figure legend, the reader is referred to the web version of this article.)

laminates do not show the left-handed behavior, i.e., $\Delta\varepsilon_{ngv} = 0$; this area is shaded in blue color.

Next, we study the evolution of dispersion relation with applied compression in the absolutely-stable composites that also exhibit NGV state. In Fig. 3, we show the frequency (a) and the group velocity $v_{gr} = \partial\omega/\partial k_1$ (b) as the function of normalized wavenumber $\tilde{k}_1 = k_1 a/(2\pi)$ in the absolutely-stable laminates with $\mu^{(f)}/\mu^{(m)} = 10$, $c^{(f)} = 0.02$, and $J_m^{(m)} = 1.1$. The frequency is normalized as $\tilde{f} = \frac{\omega a}{2\pi}\sqrt{\overline{\rho}/\tilde{\mu}}$ and the group velocity is normalized by $v_0 = \sqrt{\tilde{\mu}/\overline{\rho}}$, where $\tilde{\mu} = (c^{(m)}/\mu^{(m)} + c^{(f)}/\mu^{(f)})^{-1}$, and $\overline{\rho} = c^{(m)}\rho^{(m)} + c^{(f)}\rho^{(f)}$ is the average density.

Clearly, the dispersion relation of the shear waves propagating along the layers is highly tunable by the applied compression level. First, the relation turns non-linear at smaller compression levels (for example, at $\lambda = 0.83$), from linear in the undeformed laminate ($\lambda = 1$). The applied contraction preferably affects the shear waves with wavenumbers closer to the critical wavenumber value. For the laminate considered in Fig. 3(a), the influence becomes weak outside of the approximate range $0.0625 \lesssim 1/\tilde{k}_1 \lesssim 1$. At further higher deformation levels, for example, at $\lambda = 0.79$, the slope of the dispersion curves turns negative at certain wavenumbers, $\partial\omega/\partial k_1 < 0$, however, the frequency remains positive throughout, $\omega > 0$. This state corresponds to the appearance of NGV, which is activated via applied deformation [see the dotted curves in Fig. 3(a) and (b)]. The range of wavenumber for which the NGV is attained, Δk_{ngv}, also varies with deformation. First, the range increases with compression for $\lambda_s \lesssim 0.8$, and reaches its maximum at $\lambda \approx 0.76$. Afterwards, Δk_{ngv} decreases for $\lambda \lesssim 0.76$ and approaches $\Delta k_{ngv} = 0$ at $\lambda_e \approx 0.72$.

With further increase in the compression levels, we observe that the slope of the dispersion curves switches back to positive for all wavenumbers; for example, see the orange solid curves corresponding to $\lambda = 0.71$ in Fig. 3(a) and (b). Moreover, at even higher deformations, $\lambda = 0.67$, the non-linearity of the dispersion curve further decreases. This change in the acoustic behavior can be attributed to the significant stiffening of the matrix phase at higher deformations, which results in the decrease of effective stiffness contrast between the stiff layer and matrix phase. The variation in the sign of group velocity with compression, for the S-waves with wavenumber $\tilde{k}_1 = 5$, is also illustrated by the scale in Fig. 3(d), highlighted in color according to the direction of group velocity – green for positive and red for negative. In particular, the group velocity is negative between the deformation levels $\lambda \approx 0.8$ and $\lambda \approx 0.725$ when $\tilde{k}_1 = 5$.

Note that the appearance of the NGV state is also dictated by the wavelength of the S-waves together with the deformation level. For example, at wavenumbers $\tilde{k}_1 = 3$ and $\tilde{k}_1 = 7$, the group velocity remains positive regardless of applied deformation [see green dash-dotted and black solid curves in Fig. 3(c)]. However, for waves with $\tilde{k}_1 = 5$, the negative group velocity is induced in the deformation level range from $\lambda \approx 0.8$ to $\lambda \approx 0.725$. Recall that in the laminates that develop instability, the appearance of NGV signals the forthcoming onset of buckling with a comparable characteristic wavelength [22]. In the vicinity of critical deformation level, the NGV state indicates the existence of soft shear mode of equivalent wavelengths. In an *absolutely-stable* laminate (considered in Fig. 3), the wavenumbers at which the NGV occurs correspond to the similar soft mode that could have transitioned into the buckling of the stiff layer. However, a further compression leads to a decrease in the phase shear modulus contrast due to strong stiffening of the matrix, resulting in completely stable behavior. Moreover, in the vicinity of lock-up stretch, because of extensive increase in stiffening of matrix phase, the group velocity significantly increases irrespective of the wavenumber of shear waves; for matrix phase with $J_m^{(m)} = 1.1$, the lock-up stretch is $\lambda_{lock} = 0.605$.

Fig. 3(d) illustrates the change in the eigenmodes with applied deformation for shear waves with wavenumber $\tilde{k}_1 = 5$. The modes are plotted for the undeformed ($\lambda = 1$), moderately deformed ($\lambda = 0.76$), and highly deformed ($\lambda = 0.64$) laminates. In the undeformed state, when the group velocity is positive, the maximum amplitude of displacement occurs in the matrix phase. At the deformation level $\lambda = 0.76$, the group velocity is negative, highlighting the existence of soft shear mode that is closely related to the instability. Since laminate instability is manifested as buckling of stiff layers, in the eigenmode corresponding to NGV, we observe that comparatively larger displacement occurs in the stiff layer. However, at higher deformation levels, for example at $\lambda = 0.64$, there is a significant increase in the matrix phase stiffness due to the stiffening phenomenon. This results in LC with effectively very small stiffness contrast between the phases; the composite does not develop instability and its behavior approaches the one similar to a homogeneous material. Therefore, at this deformation level, the eigen mode has almost an equal distribution of displacement field in the layer and matrix phase, and the group velocity is positive.

Hitherto, we have shown that the NGV state can be induced in the absolutely-stable composites. Next, we investigate the deformation range for which the NGV state is active in these composites and compare it with the results of laminates that are prone to instabilities. To this end, in Fig. 4, we plot the NGV strain range $\Delta\varepsilon_{ngv}$ as the function of $J_m^{(m)}$. The results for laminates with $c^{(f)} = 0.06$ and various initial shear modulus contrasts $\mu^{(f)}/\mu^{(m)}$ are shown in Fig. 4(a), and for different volume fractions and $\mu^{(f)}/\mu^{(m)} = 10$ in Fig. 4(b). Recall that laminates with higher values of $J_m^{(m)}$ develop instabilities [see Fig. 2]; the NGV strain range $\Delta\varepsilon_{ngv} = \lambda_s - \lambda_{cr}$ in these composites is represented using filled symbols and dotted curves. However, LCs with the $J_m^{(m)}$ values smaller than the transition value are absolutely-stable; hollow symbols and solid curves show $\Delta\varepsilon_{ngv} = \lambda_s - \lambda_e$ values for these composites.

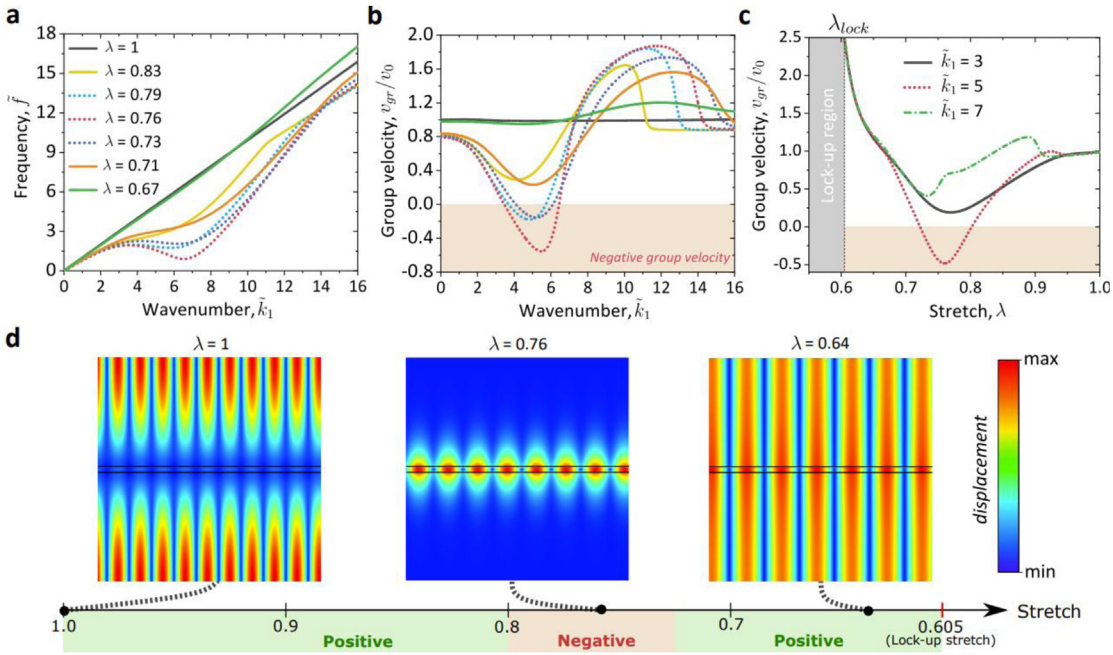

Fig. 3. Dispersion relation, group velocity $v_{gr} = \partial\omega/\partial k_1$, and eigen modes for absolutely-stable LC with $\mu^{(f)}/\mu^{(m)} = 10$, $c^{(f)} = 0.02$, and $J_m^{(m)} = 1.1$. (a) and (b) Frequency and group velocity vs the normalized wavenumber $\tilde{k}_1 = k_1 a/(2\pi)$, respectively, at different compression levels. (c) Group velocity as the function of the stretch at different wavenumbers. (d) The eigen modes corresponding to $\tilde{k}_1 = 5$ at $\lambda = 1$, 0.76, and 0.64. The color on the eigenmodes shows the relative displacement magnitude as per the color bar on right. The scale below shows the variation of group velocity's sign with stretch ratio (green – positive and red – negative). (For interpretation of the references to color in this figure legend, the reader is referred to the web version of this article.)

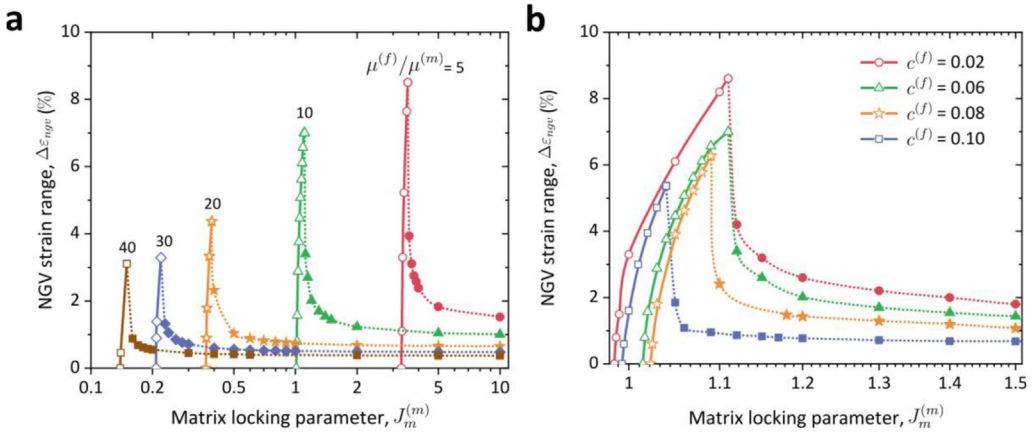

Fig. 4. NGV strain range as the functions of matrix locking parameter. Laminates with $c^{(f)} = 0.06$ (a) $\mu^{(f)}/\mu^{(m)} = 10$ (b) are considered.

Consider, for example, the laminates with shear modulus contrast $\mu^{(f)}/\mu^{(m)} = 10$ and $c^{(f)} = 0.06$ [green triangles in Fig. 4(a) and (b)]. We observe that with an increase in the matrix phase stiffening (decrease in $J_m^{(m)}$), the NGV strain range increases for the LCs that develop instabilities [see filled triangles]. Note that there is a sharp increase in $\Delta\varepsilon_{ngv}$ values close to the transition point ($J_m^{(m)} \approx 1.12$). In contrast, in composites with $J_m^{(m)}$ values smaller than transition point (corresponding to the absolutely-stable composites), the NGV strain range decreases with a decrease in $J_m^{(m)}$. Eventually, no NGV state is observed in composites with very small values of $J_m^{(m)}$. The NGV strain range attains its maximum value, $\Delta\varepsilon_{ngv}^{max}$, at matrix locking parameter just smaller than the transition value, i.e., in the absolutely-stable composites. A similar trend of $\Delta\varepsilon_{ngv}$ dependence on the matrix locking parameter is observed for every LC, regardless of their initial shear modulus contrast or volume fraction of phases [see Fig. 4(a) and (b)].

We observe that the $\Delta\varepsilon_{ngv}^{max}$ value monotonically increases with a decrease in the initial shear modulus contrast of the laminate. For example, in the laminates considered in Fig. 4(a), the ($\mu^{(f)}/\mu^{(m)}$, $\Delta\varepsilon_{ngv}^{max}$) values are: (5, 8.5%), (10, 7%), (20, 4.37%), and (40, 3.11%) [see Fig. 4(a)]. Similarly, $\Delta\varepsilon_{ngv}^{max}$ also decreases with an increase in the stiff layer volume fraction [see Fig. 4(b)]. Moreover, the value of $J_m^{(m)}$ corresponding to transition and consequently the $J_m^{(m)}$ value at which the $\Delta\varepsilon_{ngv}^{max}$ is attained also decreases with increase in $\mu^{(f)}/\mu^{(m)}$ and $c^{(f)}$. This is due to the fact that the influence of matrix phase stiffening decreases in a composite with an increase in its shear modulus contrast and stiff layer's volume fraction.

Next, we study the effect of phase densities on the NGV strain range. Fig. 5 shows the $\Delta\varepsilon_{ngv}$ dependence on the density contrast between the phases, $\rho^{(f)}/\rho^{(m)}$. In particular, the results are shown for four different classes of laminates (with morphologies defined in the caption of Fig. 5). Note that the composites (a) and (b)

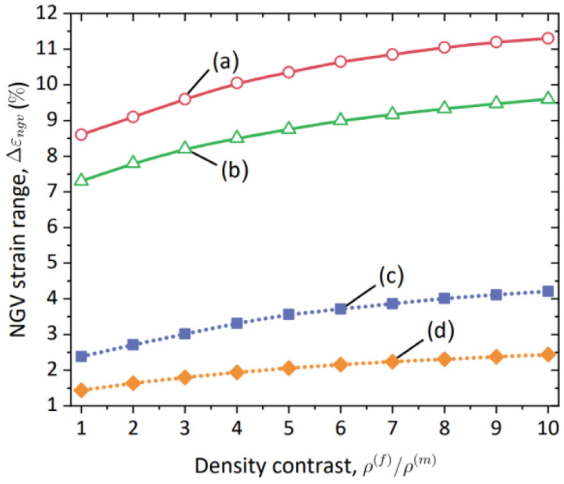

Fig. 5. NGV strain range as the function of density contrast. Four different class of laminates are considered: (a) $\mu^{(f)}/\mu^{(m)} = 10$, $c^{(f)} = 0.02$, $J_m^{(m)} = 1.11$; (b) $\mu^{(f)}/\mu^{(m)} = 10$, $c^{(f)} = 0.06$, $J_m^{(m)} = 1.11$; (c) $\mu^{(f)}/\mu^{(m)} = 5$, $c^{(f)} = 0.06$, $J_m^{(m)} = 4$; and (d) $\mu^{(f)}/\mu^{(m)} = 10$, $c^{(f)} = 0.06$, $J_m^{(m)} = 1.5$.

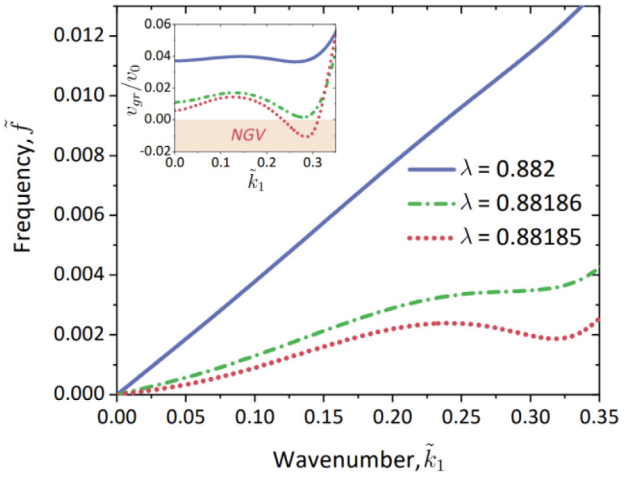

Fig. 6. Emergence of NGV state in laminate with $\mu^{(f)}/\mu^{(m)} = 15$ and $c^{(f)} = 0.13565$. This laminate develops macroscopic instability at $\lambda = 0.88184$.

are absolutely-stable composites (represented using solid lines and hollow symbols), whereas LCs (c) and (d) develop microscopic instability (dotted lines and filled symbols). As expected, the phase densities do not affect the stability characteristics of the LCs. However, the NGV strain range is significantly affected by the density contrast. We observe that $\Delta\varepsilon_{ngv}$ monotonically increases with increase in $\rho^{(f)}/\rho^{(m)}$, regardless of the composite's morphology.

Thus far, we have studied the emergence of NGV state in LCs that either are absolutely-stable or exhibit *microscopic* instability. Can the LCs developing *macroscopic* mode of instability show this left-handed behavior? We find that there exist only a few special morphologies of the composites that show the NGV state ahead of macroscopic instability. These special morphologies correspond to composites that have the material/geometric parameters in the vicinity of threshold values (where the transition in the instability mode from micro to macro takes place). For example, in neo-Hookean laminates with shear modulus contrast $\mu^{(f)}/\mu^{(m)} = 15$, the instability mode switches from microscopic to macroscopic with an increase in stiff layer volume fraction at $c_{th}^{(f)} \approx 0.135$.

As an example, consider the LC with stiff layer volume fraction slightly higher than the threshold value $c_{th}^{(f)}$, i.e., $c^{(f)} = 0.13565$ and $\mu^{(f)}/\mu^{(m)} = 15$ [see Fig. 6]; this composite develops macroscopic instability at $\lambda_{cr} = 0.88184$. However, at deformation levels preceding the critical level, we observe that, for instance, at $\lambda = 0.88186$, the dispersion curve turns non-linear. Moreover, the negative slope of the dispersion curve is observed at $\lambda = 0.88185$, which corresponds to the NGV state [see red dotted in Fig. 6 and its inset]. We note that the width of the deformation range at which the NGV state is activated is narrow, for this case, $\Delta\varepsilon_{ngv} \approx 1.5 \times 10^{-3}\%$. Arguably, from the experimental point of view, this strain range may not be detectable. Nevertheless, this allows us to conclude that composites with macroscopic instability as the primary mode of failure can also exhibit NGV state.

4. Conclusion

In summary, we have studied the emergence of the NGV state corresponding to S-waves in layered composites traveling parallel to the layers, which is the non-periodic direction. This state can be reversibly activated via compression along the layers. We find that this left-handed behavior can be evoked in the absolutely-stable laminates. Remarkably, the strain range for which group and phase velocity are anti-parallel, can be significantly higher in laminates that do not buckle. We find that with an increase in matrix phase stiffening the NGV strain range increases in laminates that develop instabilities, whereas the strain range decreases in the absolutely-stable composites. In practice, the extent of matrix stiffening may be regulated through, for example, varying the level of crosslink density [24]. For instance, the crosslink density can be controlled by the light intensity during the polymerization process of a 3D printed soft polymer [39,40]. Furthermore, designing matrix phase using the combination of polymer networks and stiff-inclusions can provide better control on its stiffening behavior [41,42]. We also find that an increase in the density contrast between the phases results in further widening of the NGV strain range (up to 11% in our examples). The enhancement can be important for realizing the deformation-activated NGV states. This unusual behavior may be further utilized in developing novel acoustic metamaterials with negative time delays and backward propagation of pulse, also known as fast light in optics [43–47].

Finally, we note that the reported dispersion relations resemble those observed for the gravity-capillary waves on the surface of stationary flowing water [48]. In particular, similar to surface waves in water at a given current velocity, in laminates subjected to certain deformation levels there exist horizons (points at which the group velocity direction reverses). For example, see Fig. 3(a), the slope of the red dotted curve switches twice: positive to negative at $\tilde{k}_1 \approx 3.5$ and turns back positive at $\tilde{k}_1 \approx 6.6$; these two (blocking) points are respectively termed as white and blue horizons (for details see Rousseaux et al. [48]). Therefore, an equally exciting prospect to investigate in future studies is that akin to surface waves on fluids, S-waves in soft composites can be potentially demonstrated as the mechanical wave analogue of the Hawking effect (black hole radiation) and/or used to simulate interstellar travels [49–52].

Declaration of competing interest

The authors declare that they have no known competing financial interests or personal relationships that could have appeared to influence the work reported in this paper.

Data availability

The data that supports the findings of this study are available within the article.

Acknowledgements

The authors are grateful for the support through the University of Wisconsin–Madison with funding from the Wisconsin Alumni Research Foundation.

References

[1] S.H. Lee, C.M. Park, Y.M. Seo, Z.G. Wang, C.K. Kim, Phys. Rev. Lett. 104 (2010) 54301.
[2] N. Kaina, F. Lemoult, M. Fink, G. Lerosey, Nature 525 (2015) 77–81.
[3] T. Brunet, J. Leng, O. Mondain-Monval, Science 342 (2013) 323–324.
[4] N. Fang, D. Xi, J. Xu, M. Ambati, W. Srituravanich, C. Sun, X. Zhang, Nature Mater. 5 (2006) 452–456.
[5] M.S. Kushwaha, P. Halevi, L. Dobrzynski, B. Djafari-Rouhani, Phys. Rev. Lett. 71 (1993) 2022–2025.
[6] P. Wang, F. Casadei, S. Shan, J.C. Weaver, K. and Bertoldi, Phys. Rev. Lett. 113 (2014) 14301.
[7] S. Zhang, C. Xia, N. Fang, Phys. Rev. Lett. 106 (2011) 24301.
[8] X.-F. Li, X. Ni, L. Feng, M.-H. Lu, C. He, Y.-F. Chen, Phys. Rev. Lett. 106 (2011).
[9] S. Rudykh, M.C. Boyce, Phys. Rev. Lett. 112 (2014) 34301.
[10] J. Li, V. Slesarenko, S. Rudykh, Soft Matter 14 (2018) 6171–6180.
[11] L. Wang, K. Bertoldi, Int. J. Solids Struct. 49 (2012) 2881–2885.
[12] S. Babaee, N. Viard, P. Wang, N.X. Fang, K. Bertoldi, Adv. Mater. 28 (2016) 1631–1635.
[13] K. Bertoldi, M.C. Boyce, Phys. Rev. B 78 (2008) 184107.
[14] W.J. Parnell, A.N. Norris, T. Shearer, Appl. Phys. Lett. 100 (2012) 171907.
[15] P.I. Galich, S. Rudykh, Appl. Phys. Lett. 107 (2015) 56101.
[16] Z. Chang, H.-Y. Guo, B. Li, X.-Q. Feng, Appl. Phys. Lett. 106 (2015) 161903.
[17] H. Godfrin, M. Meschke, H.-J. Lauter, A. Sultan, H.M. Böhm, E. Krotscheck, M. Panholzer, Nature 483 (2012) 576–579.
[18] K. Beauvois, J. Dawidowski, B. Fåk, H. Godfrin, E. Krotscheck, J. Ollivier, A. Sultan, Phys. Rev. B 97 (2018) 184520.
[19] Y. Chen, M. Kadic, M. Wegener, Nature Commun. 12 (2021) 1–8.
[20] D.R. Smith, J.B. Pendry, M.C.K. Wiltshire, Science 305 (2004) 788–792.
[21] V.M. Garcia-Chocano, J. Christensen, J. Sánchez-Dehesa, Phys. Rev. Lett. 112 (2014) 144301.
[22] V. Slesarenko, P.I. Galich, J. Li, N.X. Fang, S. Rudykh, Appl. Phys. Lett. 113 (2018) 31901.
[23] A.N. Gent, Rubber Chem. Technol. 69 (1996) 59–61.
[24] L.R.G. Treolar, 1975.
[25] N. Arora, J. Li, V. Slesarenko, S. Rudykh, Internat. J. Engrg. Sci. 157 (2020).
[26] M.S. Kushwaha, P. Halevi, G. Martinez, L. Dobrzynski, B. Djafari-Rouhani, Phys. Rev. B 49 (1994) 2313–2322.
[27] P.I. Galich, V. Slesarenko, S. Rudykh, Int. J. Solids Struct. 110–111 (2017) 294–304.
[28] M. Aberg, P. Gudmundson, J. Acoust. Soc. Am. 102 (1997) 2007–2013.
[29] G. Geymonat, S. Müller, N. Triantafyllidis, Arch. Ration. Mech. Anal. 122 (1993) 231–290.
[30] F. Greco, L. Leonetti, P. Lonetti, R. Luciano, A. Pranno, Compos. Struct. (2020) 112529.
[31] N. Triantafyllidis, B.N. Maker, Trans. ASME, J. Appl. Mech. 52 (1985) 794–800.
[32] S. Rudykh, G. deBotton, J. Elasticity 106 (2012) 123–147.
[33] N. Arora, A. Batan, J. Li, V. Slesarenko, S. Rudykh, Materials 12 (2019).
[34] J. Li, N. Arora, S. Rudykh, Curr. Opin. Solid State Mater. Sci. 25 (2021) 100898.
[35] V. Slesarenko, S. Rudykh, J. Mech. Phys. Solids 99 (2017) 471–482.
[36] J.-C. Michel, O. Lopez-Pamies, P.P. Castañeda, N. Triantafyllidis, J. Mech. Phys. Solids 58 (2010) 1776–1803.
[37] N. Triantafyllidis, M.D. Nestorović, M.W. Schraad, J. Appl. Mech. 73 (2006) 505–515.
[38] P.I. Galich, V. Slesarenko, J. Li, S. Rudykh, Internat. J. Engrg. Sci. 130 (2018) 51–61.
[39] J. Wu, Z. Zhao, C.M. Hamel, X. Mu, X. Kuang, Z. Guo, H.J. Qi, J. Mech. Phys. Solids 112 (2018) 25–49.
[40] Y. Xiang, C. Schilling, N. Arora, A.J. Boydston, S. Rudykh, Addit. Manuf. (2020) 101511.
[41] A.S.G. van Oosten, X. Chen, L. Chin, K. Cruz, A.E. Patteson, K. Pogoda, V.B. Shenoy, P.A. Janmey, Nature 573 (2019) 96–101.
[42] J.L. Shivers, J. Feng, A.S.G. van Oosten, H. Levine, P.A. Janmey, F.C. MacKintosh, Proc. Natl. Acad. Sci. 117 (2020) 21037–21044.
[43] G.M. Gehring, A. Schweinsberg, C. Barsi, N. Kostinski, R.W. Boyd, Science 312 (2006) 895–897.
[44] M. Ware, S.A. Glasgow, J. Peatross, Opt. Express 9 (2001) 519–532.
[45] S. Chu, S. Wong, Phys. Rev. Lett. 48 (1982) 738.
[46] B. Segard, B. Macke, Phys. Lett. A 109 (1985) 213–216.
[47] M.D. Stenner, D.J. Gauthier, M.A. Neifeld, Nature 425 (2003) 695–698.
[48] G. Rousseaux, P. Maissa, C. Mathis, P. Coullet, T.G. Philbin, U. Leonhardt, New J. Phys. 12 (2010) 95018.
[49] L.-P. Euvé, G. Rousseaux, Phys. Rev. D 96 (2017) 64042.
[50] G. Rousseaux, H. Kellay, Philos. Trans. R. Soc. A 378 (2020) 20190233.
[51] L.-P. Euvé, F. Michel, R. Parentani, T.G. Philbin, G. Rousseaux, Phys. Rev. Lett. 117 (2016) 121301.
[52] L.-P. Euvé, S. Robertson, N. James, A. Fabbri, G. Rousseaux, Phys. Rev. Lett. 124 (2020) 141101.